Inorg. Chem. **2006**, *45*, 6083–6093

Electron Distribution in Iron Octaethyloxophlorin Complexes. Importance of the Fe(III) Oxophlorin Trianion Form in the Bis-pyridine and Bis-imidazole Complexes

Sankar Prasad Rath,[‡] Marilyn M. Olmstead,[†] and Alan L. Balch*[,†]

Contribution from the Department of Chemistry, University of California, Davis, California 95616, and Department of Chemistry, Indian Institute of Technology Kanpur, Kanpur-208016, India

Received April 25, 2006

The apportionment of electrons between iron and the porphyrinic macrocycle in complexes of octaethyloxophlorin (H_3OEPO) has been a vexing problem. In particular, for **(**$Py)_2Fe$(OEPO), which is an important intermediate in heme degradation, three resonance structures involving Fe(III), Fe(II), or Fe(I), respectively, have been considered. To clarify this matter, the electronic and geometric structures of **(**$Py)_2Fe^{III}$(OEPO), **(**$Im)_2Fe^{III}$(OEPO)·2THF, and **(**$Im)_2Fe^{III}$(OEPO)·1.6$CHCl_3$ have been examined by single-crystal X-ray diffraction, measurement of magnetic moments as a function of temperature, and EPR and NMR spectral studies. The results clearly show that both complexes exist in the Fe(III)/oxophlorin trianion form rather than the Fe(II)/oxophlorin radical form previously established for **(**2,6-xylylNC$)_2Fe^{II}$(OEPO$^{\bullet}$). In the solid state from 10 to 300 K, **(**$Py)_2Fe^{III}$(OEPO) exists in the high-spin ($S = 5/2$) state with the axial ligands in parallel planes, a planar porphyrin, and long axial Fe–N distances. However, in solution it exists predominantly in a low-spin ($S = 1/2$) form. In contrast, the structures of **(**$Im)_2Fe^{III}$(OEPO)·2THF and **(**$Im)_2Fe^{III}$(OEPO)·1.6$CHCl_3$ consist of porphyrins with a severe ruffled distortion, axial ligands in nearly perpendicular planes, and relatively short axial Fe–N distances. The crystallographic, magnetic, EPR, and NMR results all indicate that **(**$Im)_2Fe^{III}$(OEPO) exists in the low-spin Fe(III) form in both the solid state and in solution.

Introduction

The oxidative destruction of heme in vivo or in vitro involves the initial introduction of oxygen into a meso position of the porphyrin.[1] Thus, the first intermediates in the process of heme oxidation involve iron complexes of the oxophlorin macrocycle such as those shown in Scheme 1. Identification of the electronic structure of complexes of the type {L_2Fe(OEPO)} is a complex problem which has been an issue of debate for some time.[2] As seen in Scheme 1, three resonance structures can be drawn for such a complex. These structures differ in the manner in which the electrons are apportioned between the ligand and the iron. Thus, the formulation L_2Fe^{III}(OEPO) involves a trianionic oxophlorin ligand with iron in the Fe(III) oxidation state.

Scheme 1

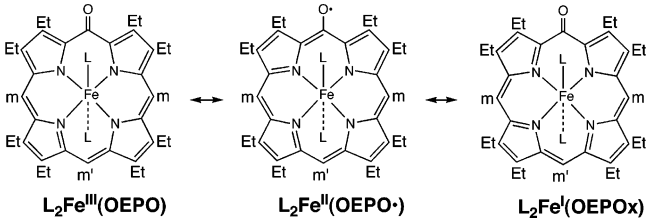

Similarly, L_2Fe^{II}(OEPO$^{\bullet}$) utilizes a dianionic ligand which is π-radical and the iron is in the Fe(II) oxidation state, and L_2Fe^{I}(OEPOx) involves a monoanionic, oxidized form of the ligand with iron in the Fe(I) oxidation state. While the earliest work on this type of complex favored the Fe(I) formulation,[3–5] more recent studies have concentrated on formulations involving either Fe(III) or Fe(II).[6–9] In addition to the issues

* To whom correspondence should be addressed.
† University of California
‡ Indian Institute of Technology Kanpur.

(1) Ortiz de Montellano; P. R. *Acc. Chem. Res.* **1998**, *31*, 543. Maines, M. D. *Heme Oxygenase: Clinical Applications and Functions*; CRC Press: Boca Raton, FL, 1992.
(2) Balch, A. L. *Coord. Chem. Rev.* **2000**, *200−202*, 349.
(3) Sano, S.; Suigura, Y.; Maeda, Y.; Ogawa, S.; Morishima, I. *J. Am. Chem. Soc.* **1981**, *103*, 2888.
(4) Sano, S.; Sano, T.; Morishima, I.; Shiro, Y.; Maeda, Y. *Proc. Natl. Acad. Sci. U.S.A.* **1986**, *83*, 531.
(5) Morishima, I.; Fujii, H.; Shiro, Y. *J. Am. Chem. Soc.* **1986**, *108*, 3858.

10.1021/ic0607033 CCC: $33.50
Published on Web 06/08/2006

Scheme 2

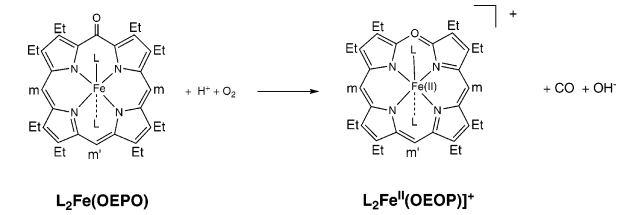

Scheme 3

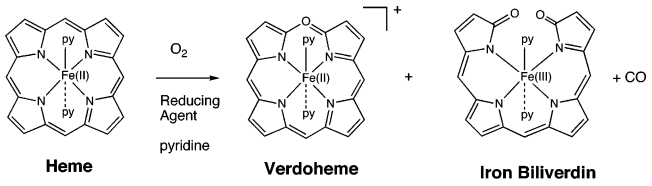

of how to apportion the electrons, the spin state of the iron is another parameter that needs to be determined for such complexes.[6,7] Finally, some of the spectroscopic studies done on complexes of this type indicate that its properties are sensitive to the availability of protons with the meso oxygen atom as the probable site of protonation.[10] However, in the complexes considered here, the meso oxygen is always present in an unprotonated state.

Complexes of the type $\{L_2Fe(OEPO)\}$ are air sensitive and readily undergo opening of the macrocyclic ligand to produce verdoheme as the initial product when exposed to air or dioxygen, as shown in Scheme 2.[11,12] The nature of the axial ligands offers some control over this process. With an isocyanide as the axial ligand, the reaction stops at the formation of verdoheme but with pyridine as the axial ligand oxidation proceeds further to form an iron biliverdin complex.[11] Moreover, $\{L_2Fe(OEPO)\}$ (L = Py) has been detected as an intermediate in the process of coupled oxidation shown in Scheme 3.[13] The coupled oxidation process involves the treatment of an iron porphyrin with dioxygen and a reducing agent such as hydrazine or ascorbic acid in a strongly coordinating medium such as pyridine solution.[13,14] This process produces verdoheme, an iron biliverdin complex, and carbon monoxide. Coupled oxidation is a convenient route for the preparation of verdoheme[15] and iron biliverdin.[16] Both types of products are formed when coupled oxidation is performed using either free hemes or heme proteins.[17−19] Coupled oxidation has also been widely considered as a model for biological heme destruction as catalyzed by heme oxygenase, since similar products and intermediates are involved in both procedures.[1]

Recently, we have demonstrated how the electronic distribution in $\{L_2Fe(OEPO)\}$ can be altered when the axial ligation changes.[7] Thus, with an isocyanide ligand present, the Fe(II) state is stabilized and the complex exists in the $(RNC)_2Fe^{II}(OEPO^{\bullet})$ form.[7,12] Crystallographic studies of $(2,6\text{-xylylNC})_2Fe^{II}(OEPO^{\bullet})$ show that it contains a planar porphyrin with Fe−N and Fe−C distances that are indicative of an Fe(II) state.[7] The magnetic moment of $(2,6\text{-xylylNC})_2Fe^{II}(OEPO^{\bullet})$ has a constant value of $1.8\mu_B$ from 4 to 350 K. The EPR spectrum of $(2,6\text{-xylylNC})_2Fe^{II}(OEPO^{\bullet})$ consists of an isotropic resonance at $g = 2.004$ with a peak-to-peak separation of 24.4 G and is indicative of the free-radical nature of the macrocyclic ligand. In contrast, with 1-methylimidazole (1-MeIm) as the axial ligands, $(1\text{-MeIm})_2Fe^{III}(OEPO)$ shows temperature-dependent properties that are indicative of the presence of Fe(III) in the complex.[7] The magnetic moment of $(1\text{-MeIm})_2Fe^{III}(OEPO)$ changes from $4.8\mu_B$ at room temperature to $1.8\mu_B$ at 100 K but then remains constant on further cooling. This behavior is indicative of a spin-state change from an $S = 1/2$ state at temperatures below 100 K to an $S = 5/2$ or spin-admixed 3/2, 5/2 state at higher temperatures. The EPR spectrum of $(1\text{-MeIm})_2Fe^{III}(OEPO)$ also changes with temperature. At 4 K, a rhombic spectrum with $g = 2.65$, 2.21, and 1.64 is observed. This spectrum is similar to those of low-spin Fe(III) porphyrins with axial imidazole or pyridine ligands in a parallel orientation. On warming, the EPR spectrum changes so that an axial spectrum is seen at 298 K with $g_\perp = 5.45$ and $g_\parallel = 2.02$. Parallel changes are also seen in the X-ray crystal structure. At 90 K, the structure reveals a planar porphyrin with two axial ligands that lie in a common plane. The in-plane Fe−N distances, 2.0163(15) and 2.0017(15) Å, and the axial Fe−N distance, 1.9904(16) Å, are indicative of the presence of a low-spin ($S = 1/2$) Fe(III) center. On warming, the structure shows a significant increase in the axial Fe−N bond, which expands from 1.9904(16) Å at 90 K to 2.199(4) Å at 296 K.

In this article, we present new experimental data relevant to the electronic structure of two other complexes of the $\{L_2Fe(OEPO)\}$ family: one with L = pyridine (Py) and the other with L = imidazole (Im). The previously available physical properties of $\{L_2Fe(OEPO)\}$ with L = Py presented a conflicting picture in regard to its electronic distribution and iron spin state. Air-sensitive crystals of the complex have previously been isolated by diffusion of diethyl ether into a pyridine solution of the dimer, $Fe_2^{III}(OEPO)_2$, under a dinitrogen atmosphere and the crystal structure determined at 143 K.[6] The in-plane Fe−N bond lengths are (2.055(2) and 2.051(2) Å, while the out-of-plane Fe−N distance is much longer, 2.265(2) Å. These distances are consistent with

(6) Balch, A. L.; Koerner, R.; Latos-Grazynski, L.; Noll, B. C. *J. Am. Chem. Soc*. **1996**, *118*, 2760.
(7) Rath, S. P.; Olmstead, M. M.; Balch, A. L. *J. Am. Chem. Soc*. **2004**, *126*, 6379.
(8) Walker, F. A. *Coord. Chem. Rev.* **1999**, *186*, 471.
(9) Walker, F. A. In *The Porphyrin Handbook*; Kadish, K. M., Smith, K. M., Guilard, R., Eds.; Academic Press: San Diego, 2000; Vol. 5, p 81.
(10) Morishima, I.; Fujii, H.; Shiro, Y.; Sano, S. *Inorg. Chem*. **1995**, *34*, 1528.
(11) Rath, S. P.; Olmstead, M. M.; Balch, A. L. *Inorg. Chem.* **2004**, *43*, 7648.
(12) Masuoka, N.; Itano, H. A. *Biochemistry* **1987**, *26*, 3672.
(13) St. Claire, T. N.; Balch, A. L. *Inorg. Chem*. **1999**, *38*, 684.
(14) Balch, A. L.; Koerner, R.; Latos-Grazynski, L.; Lewis, J. E.; St. Claire, T. N.; Zovinka, E. P. *Inorg. Chem*. **1997**, *36*, 3892.
(15) Balch, A. L.; Latos-Grazynski, L.; Noll, B. C.; Olmstead, M. M.; Szterenberg, L.; Safari, N. *J. Am. Chem. Soc*. **1993**, *115*, 1422.
(16) Balch, A. L.; Latos-Grazynski, L.; Noll, B. C.; Olmstead, M. M.; Safari, N. *J. Am. Chem. Soc*. **1993**, *115*, 9056.
(17) Hildebrand, D. P.; Tang, H.; Luo, Y.; Hunter, C. L.; Smith, M.; Brayer, G. D.; Mauk, A. G. *J. Am. Chem. Soc*. **1996**, *118*, 12909.
(18) Avila, L.; Huang, H.; Damaso, C. O.; Lu, S.; Moënne-Loccoz, P.; Rivera, M. *J. Am. Chem. Soc*. **2003**, *125*, 4103.
(19) Rodríguez, J. C.; Rivera, M. *Biochemistry* **1998**, *37*, 18082.

Table 1. Selected Bond Lengths (Å) and Bond Angles (deg) for $(Py)_2Fe^{III}(OEPO)$

	$(Py)_2Fe^{III}(OEPO)$	$(Py)_2Fe^{III}(OEPO)$	$(Py)_2Fe^{III}(OEPO)^a$
temperature, K	10(2)	90(2)	143(2)
	Bond Lengths, Å		
Fe−N1	2.0447(13)	2.0476(18)	2.055(2)
Fe−N2	2.0431(13)	2.0448(18)	2.051(2)
Fe−N3	2.2351(15)	2.2432(19)	2.265(2)
C1−O5	1.288(4)	1.279(5)	1.289(4)
C10−O2	1.336(11)	1.316(17)	1.340(13)
	Bond Angles, deg		
N1−Fe−N2	89.29(5)	89.21(7)	89.13(7)
N1−Fe−N3	89.09(5)	88.97(7)	88.94(6)
N2−Fe−N3	91.08(5)	90.93(7)	91.02(7)

[a] Data from ref 6.

the presence of iron in a high-spin state but they do not in themselves distinguish between Fe(II) or Fe(III). However, in pyridine solution, the complex has a magnetic moment of 2.4 μ_B at 23 °C,[5] which suggests the presence of only a single unpaired electron and the likely possibility of the presence of low-spin Fe(III). The complex shows no EPR spectrum at room temperature in pyridine solution but shows an axial spectrum with $g_\perp = 2.31$ and $g_\parallel = 1.75$ when frozen at 77 K.[5] Low-spin Fe(III) porphyrins with axial spectra of this sort (Type III spectra in the classification of Walker[8]) have the less common $(d_{yz},d_{xz})^4(d_{xy})^1$ ground state. Thus, the EPR data also suggest the presence of a low-spin Fe(III). The ^{1}H NMR spectrum of this complex, which has two meso resonances in the far upfield region and methylene resonances that exhibit both upfield and downfield hyperfine shifts, is unusual.[10,20] This pattern has suggested that there is a significant contribution from a ligand-based radical. The variable-temperature ^{1}H NMR spectrum shows non-Curie behavior that may result from either a change in the electronic distribution or a change in the spin state at different temperatures. The ^{1}H NMR spectrum of this complex has also been interpreted in terms of a low-spin $(d_{yz},d_{xz})^4(d_{xy})^1$ ground state for the iron.[8]

Results

Preparation of Compounds. Crystals of $(Py)_2Fe^{III}(OEPO)$ were prepared by dissolution of $Fe_2^{III}(OEPO)_2$[21,22] in dioxygen-free pyridine, filtration, and subsequent layering of the resulting solution with diethyl ether under a purified dinitrogen atmosphere. The six-coordinate product is stable in the solid state and in solution as long it is protected from atmospheric dioxygen. Addition of imidazole to a slurry of $Fe_2^{III}(OEPO)_2$ in tetrahydrofuran (THF) under a dinitrogen atmosphere also resulted in the gradual dissolution of the dimer. After filtration, the solution was layered with *n*-hexane and crystals of $(Im)_2Fe^{III}(OEPO)\cdot 2THF$ slowly grew. Crystals of $(Im)_2Fe^{III}(OEPO)\cdot 1.6CHCl_3$ were prepared similarly from chloroform solution.

Variable-Temperature Single-Crystal X-ray Diffraction of $(Py)_2Fe^{III}(OEPO)$. The crystal structure of $(Py)_2Fe^{III}$(OEPO) has been investigated at 10 and 90 K in addition to the work previously published at 143 K.[6] Comparative data are given in Table 1. At all temperatures, the crystals belong to the space group $P\bar{1}$, and the iron atom is located at a center of symmetry. Figure 1 shows a drawing of the structure from the data obtained at 10 K. The structures at other temperatures are similar as the data in Table 1 show. As Figure 1 shows, the porphyrin macrocycle is planar.

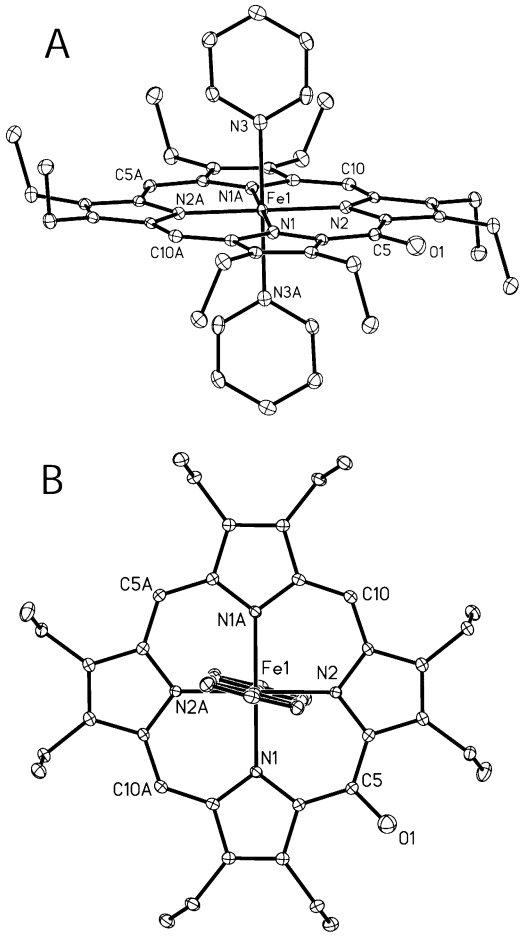

Figure 1. (A) Perspective view of $(Py)_2Fe^{III}(OEPO)$ showing 50% thermal contours from the data taken at 10 K. Only one of the four sites for the oxygen atom is shown. Site O1 has a fractional occupancy of 0.39, while site O2, which is attached to C10, has an occupancy of 0.11. Since there is a center of symmetry at the iron atom, there are also sites of oxygen atom occupation attached to C5A and C10A. (B) A view of the same molecule looking down on the porphyrin plane and showing the relative orientations of the two axial ligands.

(20) Kalish, H. R.; Latos-Grazynski, L.; Balch, A. L. *J. Am. Chem. Soc.* **2000**, *122*, 12478.
(21) Balch, A. L.; Latos-Grazynski, L.; Noll, B. C.; Olmstead, M. M.; Zovinka, E. P. *Inorg. Chem.* **1992**, *31*, 2248.
(22) Lee, H. M.; Olmstead, M. M.; Gross, G. G.; Balch, A. L. *Cryst. Growth Des.* **2003**, *3*, 691.

The iron ion is six-coordinate with two axial pyridine ligands that lie in a common plane. At 90 K, the axial Fe−N bond distance, 2.2432(19) Å, is significantly longer than the two in-plane Fe−N distances, 2.0448(18) and 2.0476(18) Å, as it is at 10 and 143 K. These Fe−N distances fall in the range found for high-spin, six-coordinate iron(III) porphyrins.[23] For example, in high-spin (2-MeIm)$_2$Fe^{III}(OEP), the in-plane Fe−N distances are 2.049(1) and 2.033(1) Å, while the out-of-plane Fe−N distance is 2.275(1) Å.[24] Like (Py)$_2$Fe^{III}(OEPO), (2-MeIm)$_2$Fe^{III}(OEP) has a centrosymmetric structure with a planar porphyrin and two axial ligands lying in a common plane. The structural parameters for (Py)$_2$Fe^{III}(OEPO) can also be compared with those of (3-Cl−Py)$_2$Fe^{III}(OEP) in its high-spin form.[25] The latter is also a centrosymmetric complex, but one which undergoes a spin equilibrium. At 293 K, there is 55% population of the high-spin form of (3-Cl-Py)$_2$Fe^{III}(OEP) in the crystal. At this temperature, the structure has been resolved into two forms, a high- and low-spin form with differing axial Fe−N distances. For the high-spin form of (3-Cl−Py)$_2$Fe^{III}(OEP), the resolved axial Fe−N distance is 2.316 Å, while the unresolved in-plane distances are 2.011(1) and 2.017(1) Å.

Comparison of the structure of (Py)$_2$Fe^{III}(OEPO) with the structure of (1-MeIm)$_2$Fe^{III}(OEPO) is particularly relevant. Both complexes crystallize in the space group $P\bar{1}$ with the iron ion located on a center of symmetry and the two axial ligands lying in parallel planes. At 90 K, however, the axial Fe−N3 distance in (1-MeIm)$_2$Fe^{III}(OEPO) is very slightly *shorter*, 1.9904(16) Å, than the in-plane Fe−N distances, 2.0163(15) and 2.0017(15) Å, while in (Py)$_2$Fe^{III}(OEPO), the axial Fe−N distance, 2.2432(19) Å, is longer than the in-plane Fe−N distances, 2.0448(18) and 2.0476(18) Å. Moreover, all the Fe−N distances in (1-MeIm)$_2$Fe^{III}(OEPO) are significantly shorter than those reported here for (Py)$_2$Fe^{III}(OEPO). The structural parameters found for (1-MeIm)$_2$Fe^{III}(OEPO) are similar to those of low-spin ($S = 1/2$), six-coordinate iron(III) porphyrins such as [(1-MeIm)$_2$Fe^{III}(TPP)]ClO$_4$ with in-plane Fe−N distances of 1.969(3), 1.988(3), 1.969(3), and 1.993(3) Å and axial Fe−N distances of 1.978(3) and 1.970(3) Å)[26] that have parallel or nearly parallel axial imidazole ligands. While the structural parameters for (Py)$_2$Fe^{III}(OEPO) indicate that it has a high-spin structure at all temperatures examined, the structure of (1-MeIm)$_2$Fe^{III}(OEPO) undergoes significant changes upon warming above 90 K that result in lengthening of the axial Fe−N bond. These changes have been discussed in the context of a reversible spin-state change involving an $S = 1/2$ state at temperatures below 100 K and population of an $S = 5/2$ or an admixed $S = 3/2$, 5/2 spin state at higher temperatures.[7]

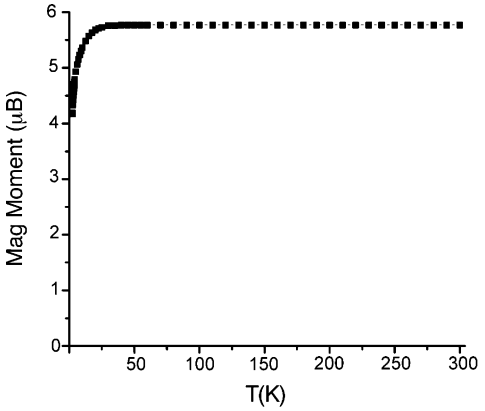

Figure 2. Magnetic moment of a polycrystalline sample of (Py)$_2$Fe^{III}(OEPO) as a function of temperature.

Since crystalline (Py)$_2$Fe^{III}(OEPO) is centrosymmetric, the position of the oxygen atom is disordered. The major site, which is the one shown in Figure 1, has 0.39 occupancy, and there is a second oxygen atom bound to the opposite side of the porphyrin also with 0.39 occupancy. The C−O distance at these sites is 1.288(4) Å at 10 K. Oxygen atoms are also located at the other two meso sites (C10 and C10A) with fractional occupancies of 0.11 at each site. In these, the C−O distance is 1.336(11) Å. This sort of disorder in the positioning of small functional groups at meso positions in substituted octaethylporphyrins is commonly encountered in their crystal structures. For example, (1-MeIm)$_2$Fe^{III}(OEPO),[7] (2,6-xylylNC)$_2$Fe^{II}(OEPO$^{\bullet}$),[7] ClFe^{III}(*meso*-NC−OEP),[27] and Zn^{II}(OEPO$^{\bullet}$)[28] show similar disorder.

Magnetic Moment of (Py)$_2$Fe^{III}(OEPO). At temperatures above 50 K, the magnetic moment of a polycrystalline sample of (Py)$_2$Fe^{III}(OEPO) is 5.9 μ_β. The magnetic moment as a function of temperature is plotted in Figure 2. The magnetic behavior follows the general form expected for high-spin complexes iron(III) porphyrin complexes with a large zero-field splitting.[29]

EPR Spectra of (Py)$_2$Fe^{III}(OEPO). The EPR spectrum of a polycrystalline sample of (Py)$_2$Fe^{III}(OEPO) at 4 K is shown in Figure 3. The spectrum is of an axial type with $g_\perp = 5.86$ and $g_\parallel = 2.06$. Similar axial spectra have been observed for other high-spin, six-coordinate Fe(III) porphyrins such as [(H$_2$O)$_2$Fe^{III}(TPP)]$^+$ ($g_\perp = 6$, $g_\parallel = 2$)[30] and [(dimethyl sulfoxide)$_2$Fe^{III}(TPP)]$^+$ ($g_\perp = 6.09$, $g_\parallel = 2.00$).[31] Thus, the EPR, magnetic moment measurements, and crystallographic results are all in agreement that (Py)$_2$Fe^{III}(OEPO) exists in a high-spin ($S = 5/2$) state in the crystalline state.

However, the EPR spectrum of the complex dissolved in pyridine differs from that seen in trace A of Figure 3. As

(23) Scheidt, W. R. In *The Porphyrin Handbook*; Kadish, K. M., Smith, K. M., Guilard, R., Eds.; Academic Press: New York, 2000; Vol 3, p 49.
(24) Geiger, D. K.; Lee, Y. J.; Scheidt, W. R. *J. Am. Chem. Soc.* **1984**, *106*, 6339.
(25) Scheidt, W. R.; Geiger, D. K.; Haller, K. J. *J. Am. Chem. Soc.* **1982**, *104*, 495.
(26) Higgins, T. B.; Safo, M. K.; Scheidt, W. R. *Inorg. Chim. Acta* **1990**, *178*, 261.
(27) Kalish, H.; Camp, J.: Stepien, M.; Latos-Grazynski, L.; Balch, A. L. *Inorg. Chem.* **2002**, *41*, 989.
(28) Balch, A. L.; Noll, B. C.; Zovinka, E. P. *J. Am. Chem. Soc.* **1991**, *114*, 3380.
(29) Mitra, S. In *Physical Bioinorganic Chemistry- Iron Porphyrins, Part II*; Lever, A. B. P., Gray, H. B., Eds.; Addison-Wesley: Reading, MA, 1983; p 1.
(30) Scheidt, W. R.; Cohen, I. A.; Kastner, M. E. *Biochemistry* **1979**, *16*, 3546.
(31) Mashiko, T.; Kastner, M. E.; Spartalian, K.; Scheidt, W. R.; Reed, C. A. *J. Am. Chem. Soc.* **1978**, *100*, 6354.

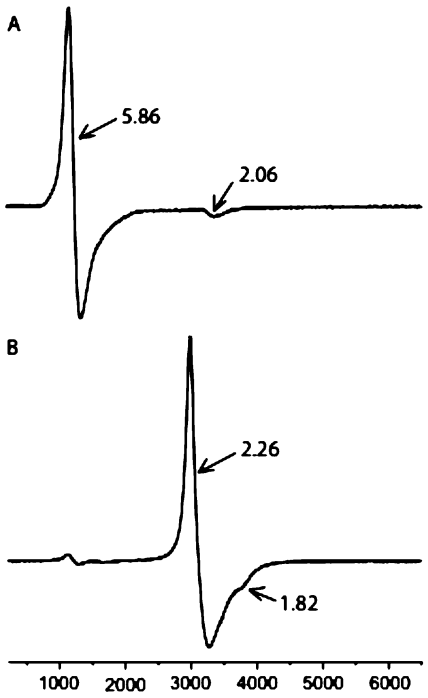

Figure 3. EPR spectra of (A) a polycrystalline sample of $(Py)_2Fe^{III}(OEPO)$ at 4 K and (B) a frozen solution of $(Py)_2Fe^{III}(OEPO)$ in pyridine at 4 K.

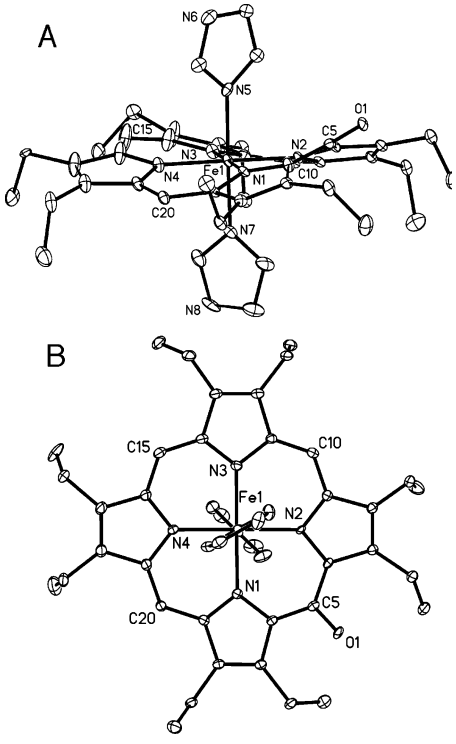

Figure 4. (A) Perspective views of Molecule 1 of $(Im)_2Fe^{III}(OEPO)\cdot 2THF$ showing 35% thermal contours. Only the major orientations, which have 0.65 site occupancies, are shown for the two ethyl groups containing C31and C33 that are affected by disorder. (B) A view of the same molecule looking down on the porphyrin plane and showing the relative orientations of the two axial ligands.

seen in trace B of Figure 3, the spectrum obtained in a frozen pyridine solution of $(Py)_2Fe^{III}(OEPO)$ at 4 K shows a different axial spectrum with substantially smaller g values: $g_\perp = 2.26$ and $g_{||} = 1.82$. Similarly, Morishima and co-workers reported $g_\perp = 2.31$ and $g_{||} = 1.79$ (at 77 K) for

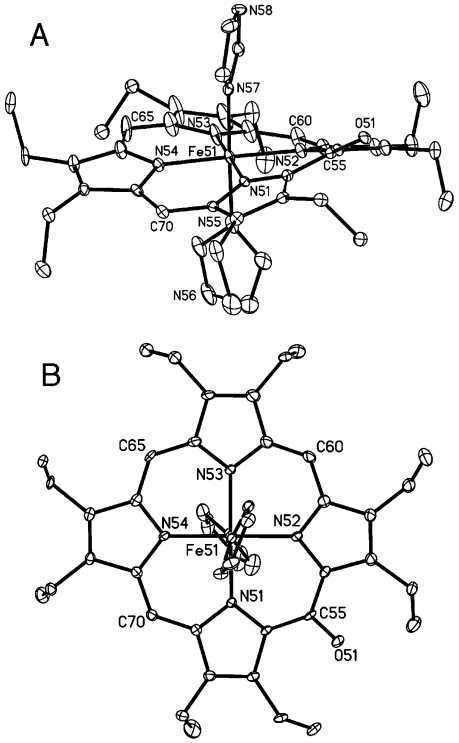

Figure 5. (A) Perspective views of Molecule 2 of $(Im)_2Fe^{III}(OEPO)\cdot 2THF$ showing 35% thermal contours. Only the major orientations, which have 0.70 site occupancies, are shown for the two ethyl groups containing C79, C 81, and C83 that are affected by disorder. (B) A view of the same molecule looking down on the porphyrin plane and showing the relative orientations of the two axial ligands.

a sample of this complex obtained by hydrolysis of (benzyloxy-OEP)$Fe^{III}Cl$ in pyridine solution.[5,10] Consequently, from the differences in the EPR spectra, it is clear that the electronic structure of $(Py)_2Fe^{III}(OEPO)$ in the solution is different from its electronic structure in the solid state.

Single-Crystal X-ray Diffraction of $(Im)_2Fe^{III}(OEPO)\cdot 2THF$. This complex crystallizes with two independent molecules in the asymmetric unit. Selected bond distances and angles are given in Table 2. Figure 4 shows two views of Molecule 1, while Figure 5 shows similar drawings of Molecule 2. The iron is six-coordinate in each, and both porphyrins have similar distortions (vide infra). The two molecules are thus similar in their core structures but differ in the positioning of the axial ligands and of the ethyl substituents.

The Fe−N bond lengths fall into rather narrow ranges: 1.957(3)−1.979(3) Å for Molecule 1 and 1.984(3)−1.964-(3) Å for Molecule 2. These distances are consistent with the presence of low-spin ($S = 1/2$) Fe(III). For comparison, $[(Im)_2Fe^{III}(OEP)]^+$ has in-plane Fe−N distances of 2.003(2) and 2.005(3) Å and an axial Fe−N distance of 1.975(2) Å.[32] The structure of $(Im)_2Fe^{III}(OEPO)\cdot 2THF$ can also be compared to that of $(1\text{-MeIm})_2Fe^{III}(OEPO)$ at 90 K. At this temperature, $(1\text{-MeIm})_2Fe^{III}(OEPO)$ has a low-spin ($S = 1/2$) structure with in-plane Fe−N distances of 2.0163(15) and

(32) Muthusamy Mylrajan, M.; Andersson, L. A.; Sun, J.; Loehr, T. M.; Thomas, C. S.; Sullivan, Jr., E. P.; Thomson, M. A.; Long, K. M.; Anderson, O. P.; Strauss; S. H. *Inorg. Chem.* **1995** *34*, 3953.

Table 2. Selected Bond Lengths (Å) and Bond Angles (deg) for $(Im)_2Fe^{III}(OEPO)\cdot 2THF$ and for $(Im)_2Fe^{III}(OEPO)\cdot 1.6CHCl_3$ at 90 K

	$(Im)_2Fe^{III}(OEPO)\cdot 2THF$ Molecule 1	$(Im)_2Fe^{III}(OEPO)\cdot 2THF$ Molecule 2	$(Im)_2Fe^{III}(OEPO)\cdot 1.6CHCl_3$ Molecule 1	$(Im)_2Fe^{III}(OEPO)\cdot 1.6CHCl_3$ Molecule 2
		Bond Lengths, Å		
Fe−N1	1.979(3)	1.984(3)	1.973(4)	1.970(4)
Fe−N2	1.976(3)	1.973(3)	1.977(4)	1.977(4)
Fe−N3	1.961(3)	1.970(4)	1.960(4)	1.958(4)
Fe−N4	1.957(4)	1.965(3)	1.962(4)	1.964(4)
Fe−N5	1.967(4)	1.964(4)	1.969(4)	1.985(4)
Fe−N7	1.967(4)	1.975(4)	1.959(4)	1.993(3)
C1−O5	1.284(5)	1.289(5)	1.290(5)	1.295(5)
		Bond Angles, deg		
N1−Fe−N2	89.11(13)	88.63(14)	89.07(16)	88.81(16)
N1−Fe−N3	178.65(15)	177.86(17)	178.67(19)	178.07(19)
N1−Fe−N4	90.43(14)	90.90(13)	90.47(16)	90.89(15)
N1−Fe−N5	90.91(14)	88.94(15)	90.12(16)	89.73(15)
N1−Fe−N7	87.50(14)	89.11(14)	89.42(17)	88.24(13)
N2−Fe−N3	90.35(14)	90.49(14)	90.40(17)	90.35(17)
N2−Fe−N4	179.06(15)	178.79(16)	179.10(18)	178.84(17)
N2−Fe−N5	89.71(14)	89.82(15)	90.25(17)	90.35(16)
N2−Fe−N7	89.22(14)	89.42(14)	87.78(17)	88.47(14)
N3−Fe−N4	90.09(14)	89.94(14)	90.04(17)	89.92(16)
N3−Fe−N5	90.32(15)	89.11(18)	91.02(19)	92.01(19)
N3−Fe−N7	91.26(15)	92.84(16)	89.3(2)	90.01(18)
N4−Fe−N5	91.12(15)	89.06(15)	90.52(17)	90.78(15)
N4−Fe−N7	89.94(15)	91.69(14)	91.44(17)	90.39(14)
N5−Fe−N7	178.10(14)	177.92(16)	178.01(17)	177.67(14)

Table 3. Crystal Data and Data Collection Parameters

	$(Py)_2Fe^{III}(OEPO)$	$(Py)_2Fe^{III}(OEPO)$	$(Py)_2Fe^{III}(OEPO)$ from ref 6	$(Im)_2Fe^{III}(OEPO)\cdot 2THF$	$(Im)_2Fe^{III}(OEPO)\cdot 1.6CHCl_3$
T, K	10(2)	90(2)	143(2)	90(2)	90(2)
formula	$C_{46}H_{53}FeN_6O$	$C_{46}H_{53}FeN_6O$	$C_{46}H_{53}FeN_6O$	$C_{50}H_{67}FeN_8O_3$	$C_{43.6}H_{52.6}Cl_{4.8}Fe_2N_8$
fw	761.79	761.79	761.79	883.97	930.75
color and habit	blue plate	blue plate	blue plate	red block	red block
cryst syst	triclinic	triclinic	triclinic	monoclinic	monoclinic
space group	$P\bar{1}$	$P\bar{1}$	$P\bar{1}$	$P2_1/c$	$P2_1/c$
a, Å	9.7928(6)	9.8604(12)	9.838(3)	19.682(3)	19.572(2)
b, Å	10.1780(6)	10.2419(13)	10.221(3)	18.979(3)	19.194(2)
c, Å	10.4503(7)	10.5271(13)	10.493(2)	25.052(4)	25.108(3)
α, deg	80.4650(10)	80.329(2)	99.57(2)	90	90
β, deg	89.9750(10)	90.060(3)	90.08(2)	98.886(4)	98.275(2)
γ, deg	66.3170(10)	66.255(2)	113.68(2)	90	90
V, Å^3	938.17(10)	956.5(2)	950.1(4)	9246(3)	9334.0(17)
radiation (λ, Å)	Mo Kα (0.71073)	Mo Kα (0.71073)	Mo Kα (0.71073)	Mo Kα (0.71073)	Mo Kα (0.71073)
Z	1	1	1	8	8
d_{calcd}, g·cm^{-3}	1.348	1.322	1.331	1.270	1.325
μ, mm^{-1}	0.448	0.439	0.442	0.377	0.640
no. of unique data	4306	4384	3441	18055	20360
no. of restraints	0	0	1	0	25
no. of params. refined	254	254	255	1218	1212
R1[a]	0.037	0.044	0.036	0.082	0.096
wR2[b]	0.097	0.106	0.079	0.170	0.302

[a] For data with $I > 2\sigma I$. $R1 = \sum||F_o|\sum|F_c||/\sum|F_o|$. [b] For all data. $wR2 = \sqrt{\sum[w(F_o^2\sum F_c^2)^2]/\sum[w(F_o^2)^2]}$.

2.0017(15) Å and an out-of plane Fe−N distance of 1.9904(16) Å.[7]

The two axial ligands are approximately perpendicular to one another. In Molecule 1, the dihedral angle between the least squares planes of the two axial ligands is 73.6°, while in Molecule 2 the corresponding angle is 64.7°. The imidazole ligands are arranged so that they are aligned roughly parallel to trans meso positions of the porphyrin. In Molecule 1, the angle between the plane of the imidazole ligand containing N5 and the Fe−N1 bond is −61.2° and the corresponding angle between the imidazole ring containing N7 and the Fe−N1 bond is 45.2°. In Molecule 2, the angle between the plane of the imidazole ligand containing N55 and the Fe51−N51 bond is 41.6° and the corresponding angle between the imidazole ring containing N57 and the Fe−N51 bond is −23.1°.

The porphyrin is distinctly nonplanar. The distortions of porphyrin macrocycles from planarity follow the low-frequency normal vibrational modes of the porphyrin and involve *sad*, *ruf*, *dom*, *wav*(*x*), *wav*(*y*), and *pro* deformations.[33,34] For $(Im)_2Fe^{III}(OEPO)$, there is a significant *ruf* (S_4) distortion. Figure 6 shows the out-of-plane displacements (in units of 0.01 Å) of the core atoms for each molecule in $(Im)_2Fe^{III}(OEPO)\cdot 2THF$. Both molecules show very similar distortions. This sort of distortion minimizes through-space

(33) Jentzen, W.; Song, X.-Z.; Shelnutt, J. A. *J. Phys. Chem. B* **1997**, *101*, 1684.
(34) Shelnutt, J. A.; Song, X.-Z.; Ma, J.-G.; Jia, S.-L.; Jentzen, W.; Medforth, C. J. *Chem. Soc. Rev.* **1998**, *27*, 31.

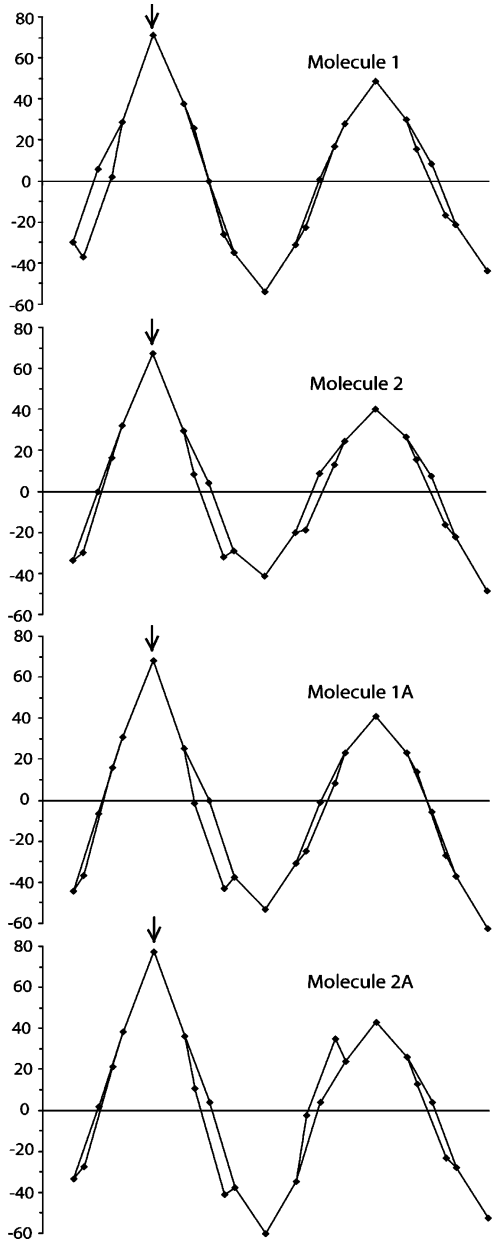

Figure 6. Diagrams comparing the out-of-plane displacements (in units of 0.01 Å) of the porphyrin core atoms from the mean plane of the porphyrin for the two independent molecules of $(Im)_2Fe^{III}(OEPO)\cdot 2THF$ (Molecule 1 and Molecule 2) and for $(Im)_2Fe^{III}(OEPO)\cdot 1.6\ CHCl_3$ (Molecule 1A and Molecule 2A). The arrows indicate the positions of the meso oxygen atoms.

contact of the axial ligands with the porphyrin and is seen for a number of low-spin Fe(III) porphyrins with axial imidazole or pyridine ligands that are aligned into nearly perpendicular arrangements.

The oxygen atoms on the porphyrin periphery are ordered in this structure as a result of hydrogen-bonding interactions. These hydrogen bonds involve axial imidazole ligands acting as H-bond donors toward the meso oxygen atoms of adjacent molecules. Figure 7 shows how molecules of the complex are connected by these hydrogen bonds. Both of the independent molecules in $(Im)_2Fe^{III}(OEPO)\cdot 2THF$ are involved in this hydrogen-bonded arrangement. Hydrogen bonding has served in several other related complexes (e.g., $(Py)Zn^{II}(OEPOH\cdots Py)$,[28] $BrFe^{III}(OEPO^{\bullet})CHCl_3$)[15]) to produce ordered arrangements of the peripheral meso oxo and hydroxo substituents.

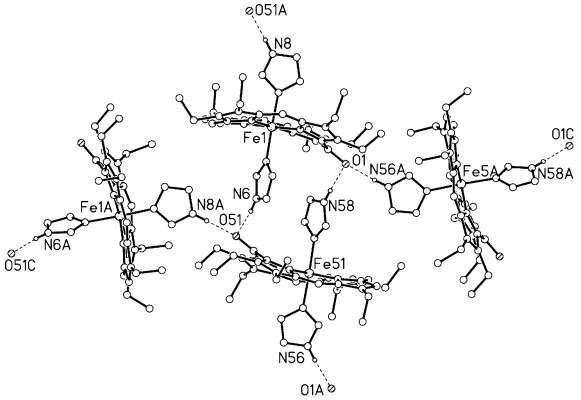

Figure 7. View of the structure of $(Im)_2Fe^{III}(OEPO)\cdot 2THF$ that shows the hydrogen bonding interactions between the porphyrins and their axial ligands. H-bonding parameters are: O1···N56A, 2.727(5); O1···N58, 2.767(5); O51···N6,2.725(5); O51···N8A, 2.747(5) Å.

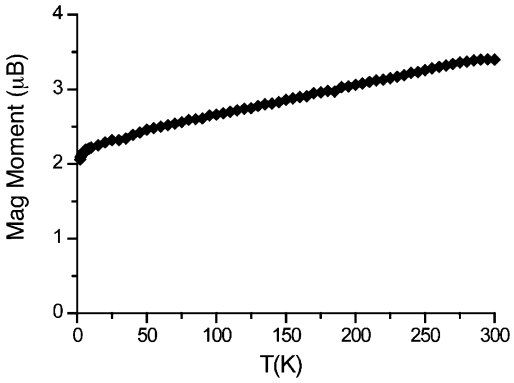

Figure 8. Magnetic moment of a polycrystalline sample of $(Im)_2Fe^{III}(OEPO)\cdot 2THF$ as a function of temperature.

While there is no disorder in the position of the meso oxygen atoms in this structure, there is some disorder in the position of the ethyl substituents. For Molecule 1, two of the ethyl groups have alternate locations. In Molecule 2, there are three ethyl groups that show similar disorder.

The crystal structure of $(Im)_2Fe^{III}(OEPO)\cdot 1.6CHCl_3$ is isostructural with that of $(Im)_2Fe^{III}(OEPO)\cdot 2THF$. Thus, there are two molecules in the asymmetric unit, both show a *ruf* distortion of the porphyrin, and both have the axial ligands lying in nearly perpendicular planes. The out-of plane displacements for $(Im)_2Fe^{III}(OEPO)\cdot 1.6CHCl_3$ are shown in Figure 6. The Fe−N distances, which are reported in Table 2, are similar to those for $(Im)_2Fe^{III}(OEPO)\cdot 2THF$. Thus, the geometry and distortion of this complex are intrinsic to the molecule itself and not a consequence of molecular packing. The hydrogen-bonding pattern seen in Figure 7 for $(Im)_2Fe^{III}(OEPO)\cdot 2THF$ is also found in $(Im)_2Fe^{III}(OEPO)\cdot 1.6CHCl_3$. Details are given in the Supporting Information.

Magnetic Moment of $(Im)_2Fe^{III}(OEPO)\cdot 2THF$. The magnetic moment of a polycrystalline sample of $(Im)_2Fe^{III}(OEPO)\cdot 2THF$ as a function of temperature is shown in Figure 8. At the lowest temperatures, the moment approaches 2.0 μ_B, which is appropriate for a low-spin ($S = 1/2$) Fe(III) complex. Increasing the temperature results in a gradual increase in the magnetic moment. This increase can arise

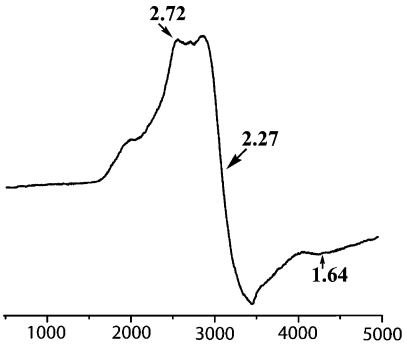

Figure 9. EPR spectrum of a polycrystalline sample of $(Im)_2Fe^{III}(OEPO)\cdot 2THF$ at 4 K.

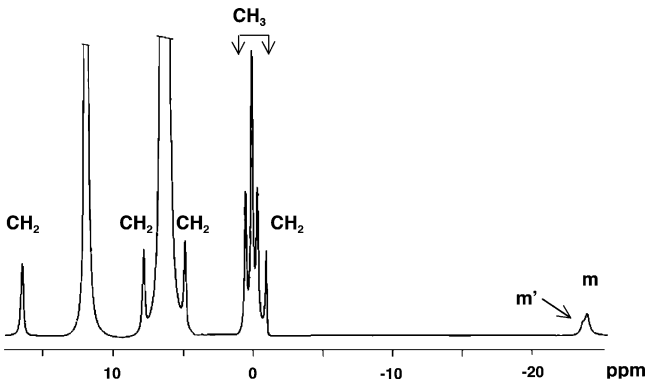

Figure 10. 400 MHz ^{1}H NMR spectrum of $(Im)_2Fe^{III}(OEPO)\cdot 2THF$ at 295 K in chloroform-*d* solution in the presence of an excess of imidazole. Resonance assignments: m, m′ meso protons, CH_2, methylene protons; CH_3, methyl protons of the ethyl groups. The intense resonances that have been truncated arise from the solvent and the excess imidazole used.

from the population of a second spin state (as is the case with $(1\text{-MeIm})_2Fe^{III}(OEPO)$[7]) or from cooperative interactions between the complexes.

EPR Spectrum of $(Im)_2Fe^{III}(OEPO)\cdot 2THF$. The EPR spectrum of a polycrystalline sample of $(Im)_2Fe^{III}(OEPO)\cdot 2THF$ at 4 K is shown in Figure 9. The spectrum is of a rhombic type with $g_3 = 2.72$, $g_2 = 2.27$, and $g_1 = 1.64$. These values are similar to those reported by Morishima and co-workers ($g_3 = 2.80$, $g_2 = 2.28$, and $g_1 = 1.57$) for a frozen solution of $(Im)_2Fe^{III}(OEPO)$ in chloroform in the presence of excess imidazole. Such spectra are typical for low-spin ($S = 1/2$) iron porphyrins with two axial imidazole ligands. However, with 4-fold symmetric porphyrins, the appearance of a rhombic spectrum of this sort for a low-spin Fe(III) complex is usually taken to indicate that the two axial ligands reside in a common plane.[8] Low-spin Fe(III) porphyrins with planar axial ligands in perpendicular orientations typically display 'large g_{max}' EPR spectra that are indicative of the near degeneracy of the d_{xz} and d_{yz} orbitals. However, in $(Im)_2Fe^{III}(OEPO)$, the intrinsic asymmetry in the oxophlorin-derived macrocycle lowers the symmetry so that a rhombic spectrum is observed, even though there is a nearly perpendicular orientation of the axial ligands.

^{1}H NMR Spectrum of $(Im)_2Fe^{III}(OEPO)\cdot 2THF$. The ^{1}H NMR spectrum of $(Im)_2Fe^{III}(OEPO)\cdot 2THF$ in chloroform-*d* solution in the presence of an excess of imidazole at room temperature is shown in Figure 10. (A similar spectrum was obtained when crystals of $(Im)_2Fe^{III}(OEPO)\cdot 1.6CHCl_3$ were dissolved in chloroform-*d*.) The spectrum consists of two closely spaced resonances of the meso protons in the upfield region, four equally intense methylene resonances in the 17 to −2 ppm range, and three methyl resonances in a 1:2:1 intensity ratio in the 1 to −1 ppm range. This pattern of resonances is similar to that obtained for a number of low-spin, meso-substituted Fe(III) porphyrins such as $[(NC)_2Fe^{III}(\textit{meso}\text{-MeO}-\text{OEP})]^-$,[27] except that the meso resonances have a somewhat larger than normal upfield shift and one of the methylene resonances has slight upfield shift. Overall, however, the spectrum is consistent with a low-spin Fe(III), six-coordinate complex with the less common $(d_{yz},d_{xz})^4(d_{xy})^1$ ground state. Previously, we have noted that low-spin complexes of the type $[(NC)_2Fe^{III}(\textit{meso}\text{-R}-\text{OEP})]^-$ have ^{1}H NMR spectra that are also indicative of this $(d_{yz},d_{xz})^4(d_{xy})^1$ ground state.[26]

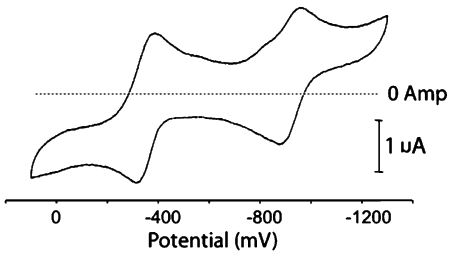

Figure 11. Cyclic voltammogram for a solution of $(Im)_2Fe^{III}(OEPO)\cdot 2THF$ in dichloromethane prepared by treating $Fe_2^{III}(OEPO)_2$ with a 10-fold excess of imidazole. The supporting electrolyte was 0.10 M tetra(*n*-butyl)ammonium perchlorate and the reference electrode was Ag/0.010 M $AgClO_4$.

Comparison of the Electrochemical Behavior of $(Py)_2Fe^{III}(OEPO)$, $(Im)_2Fe^{III}(OEPO)$, and $(N\text{-MeIm})_2Fe^{III}(OEPO)$. Figure 11 shows a cyclic voltammogram from a solution of $(Im)_2Fe^{III}(OEPO)$ in dichloromethane with an excess of imidazole and with 0.10 M tetra(*n*-butylammonium) perchlorate as supporting electrolyte. The reference electrode was silver/0.010 M $AgClO_4$. The ferrocene/ferrocenium process occurs at +220 mV in this solvent/supporting electrolyte system. A nearly reversible oxidation occurs at −0.346 mV with $\Delta E_p(\text{red}) - E_p(\text{ox}) = 68$ mV, and a reversible reduction occurs at −0.923 mV with $\Delta E_p(\text{red}) - E_p(\text{ox}) = 68$ mV. The electrochemical behavior of $(N\text{-MeIm})_2Fe^{III}(OEPO)$ is similar: oxidation at −0.332(60) with $\Delta E_p(\text{red}) - E_p(\text{ox}) = 60$ mV and reduction at −0.992(72) with $\Delta E_p(\text{red}) - E_p(\text{ox}) = 72$ mV. Under similar conditions, the oxidation of $(Py)_2Fe^{III}(OEPO)$ occurs at a significantly less negative potential, −0.190 mV with $\Delta E_p(\text{red}) - E_p(\text{ox}) = 67$ mV, but the reduction occurs at more negative potential −1.022 mV with $\Delta E_p(\text{red}) - E_p(\text{ox}) = 62$ mV. These results indicate that despite their differences the three complexes $(Py)_2Fe^{III}(OEPO)$, $(Im)_2Fe^{III}(OEPO)$, and $(N\text{-MeIm})_2Fe^{III}(OEPO)$ all undergo facile oxidation to form a monocation and a reduction to form an anion. The nature of the axial ligand does significantly influence the potential of both the oxidation and the reduction of these oxophlorin complexes.

Discussion

Electronic Distribution in $(Py)_2Fe^{III}(OEPO)$ and $(Im)_2Fe^{III}(OEPO)$. The physical characteristics reported here

for both $(Py)_2Fe^{III}$(OEPO) and $(Im)_2Fe^{III}$(OEPO) indicate that iron is present in the Fe(III) oxidation state in each complex. For example, both display anisotropic EPR spectra with g values significantly different from the free radical type spectrum at $g = 2.004$ seen for $(2,6\text{-xylylNC})_2Fe^{II}$(OEPO$^{\bullet}$).[7]

In the solid state, $(Py)_2Fe^{III}$(OEPO) exists in a high-spin ($S = 5/2$) state at all temperatures, as indicated by the crystallographic, magnetic, and EPR results. However, its electronic structure in solution is another matter. The EPR spectra (see Figure 3B and ref 9) and magnetic susceptibility ($2.4\mu_B$ at 23 °C)[5] are indicative of a low-spin ($S = 1/2$) state in solution.

The EPR spectra of low-spin, six-coordinate Fe(III) hemes have been divided into three types.[8,35,36] Type I complexes exhibit "large g_{max}" EPR spectra where one prominent resonance at $g \geq 3.2$ dominates the spectrum.[37−39] Such complexes have a $(d_{xy})^2(d_{xz},d_{yz})^3$ electronic configuration. If planar axial ligands are present, these ligands are arranged so that their planes are nearly perpendicular in Type I complexes. Type II porphyrin complexes have rhombic EPR spectra. These also have a $(d_{xy})^2(d_{xz},d_{yz})^3$ electronic configuration, but, with planar axial ligands, the ligand planes are nearly parallel. Finally, Type III hemes have axial EPR spectra with $g_{\perp} \approx 2.6$. Complexes of this type have the less common $(d_{xz},d_{yz})^4(d_{xy})^1$ electronic ground state.

In that regard, the axial EPR spectrum obtained in a frozen pyridine solution of $(Py)_2Fe^{III}$(OEPO) with $g_{\perp} = 2.26$ and $g_{||} = 1.82$ is similar to that of $[(t\text{-BuNC})_2Fe^{III}(OEP)]^+$, which has $g_{\perp} = 2.28$ and $g_{||} = 1.83$.[39] Thus, if $(Py)_2Fe^{III}$(OEPO) were a 4-fold symmetric porphyrin, the EPR spectrum of $(Py)_2Fe^{III}$(OEPO) would fall into Class III, where the less common $(d_{yz},d_{xz})^4(d_{xy})^1$ ground state is involved.[8] However, with the added meso substituent present, it is unclear exactly what factors are needed to bring about the accidental degeneracy that produces such an axial spectrum.

The non-Curie behavior of the ^{1}H NMR spectrum indicates that another spin state may also be populated when $(Py)_2Fe^{III}$(OEPO) is dissolved in pyridine. Alternatively, there may be a temperature-dependent shift in the degree of electron transfer between the iron and the porphyrin. The unusual hyperfine shift pattern in the ^{1}H NMR spectrum, with strong upfield hyperfine shifts for the two meso resonances (which appear at −118 and −160 ppm) and methylene resonances with both upfield and downfield shifts,[5,10,20] suggests that there is a significant contribution of spin that is transferred to porphyrin. The highest occupied molecular orbital of the oxophlorin trianion is a π-type orbital shown in Scheme 4, where the sizes of the circles surrounding the ligand atoms show the relative electron density coefficients at each core

Scheme 4

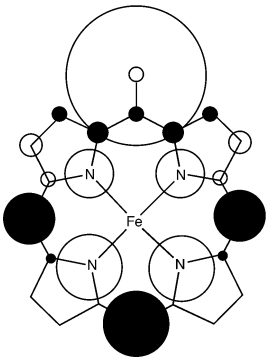

atom.[5,15] The orbital shown in Scheme 4 corresponds to the well-known porphyrin $3a_{2u}$ orbital. If there is a significant degree of electron transfer from the ligand to iron, then electron density will be removed from this orbital. As a result, there will be spin density in this ligand orbital, which has a large amplitude at the meso positions. The resulting spin density will cause large hyperfine shifts for the meso protons as has been observed for $(Py)_2Fe^{III}$(OEPO).

The factors that affect the conversion of $(Py)_2Fe^{III}$(OEPO) from a high-spin state in the solid to a low-spin state in solution deserve comment. First, it is important to note that other porphyrin complexes do show changes in spin state depending upon whether the compound is present as a solid or in solution. Thus, $[(2\text{-MeIm})_2Fe^{III}(OEP)](ClO_4)$ exists as a near-high-spin complex in the solid but undergoes temperature-dependent changes in the magnetic moment that are indicative of a $S = 1/2$, $S = 5/2$ equilibrium in solution.[24] Likewise, $[(2\text{-MeIm})_2Fe^{III}(TPP)](ClO_4)$ exists in the low-spin form in the solid, but again, it dissolves to produce an equilibrium between the $S = 1/2$ and $S = 5/2$ states in solution.[24] For $(Py)_2Fe^{III}$(OEPO), it may be that the orientation of the axial ligands needs to be altered from that seen in the solid state to accommodate a transformation to a low-spin form. In the solid state, the axial ligands are arranged in a parallel arrangement that nearly eclipses a trans set of Fe−N(porphyrin) bonds. Any twisting of the ligands about the Fe−N bonds is clearly inhibited in the solid state, but reorientation becomes feasible when the molecule is dissolved. Such reorientation of the axial ligands can alleviate overlap of the axial ligand with the porphyrin and can facilitate the shortening of the axial Fe−N bonds that is needed to form the low-spin state. With $(1\text{-MeIm})_2Fe^{III}$(OEPO), such twisting is unnecessary since the five-membered imidazole ring offers less steric hindrance to Fe−N bond shortening.

For $(Im)_2Fe^{III}$(OEPO), the crystallographic and spectroscopic data indicate that an $S = 1/2$ state Fe(III) state is present both in the solid and in solution. The gradual increase in the magnetic moment with temperature in the solid state may indicate that a higher spin state is occupied at higher temperatures or may result from cooperative interactions between the hydrogen-bonded hemes. In solution, the EPR and NMR spectral data are indicative of the presence of a low-spin state as well.

(35) Yatsunyk, L. A.; Carducci, M. D.; Walker, F. A. *J. Am. Chem. Soc.* **2003**, *125*, 15986.
(36) Benda, R.; Schünemann, V.; Trautwein, A. X.; Sheng Cai, S.; Polam, J. R.; Watson, C. T.; Shokhireva, T. Kh.; Walker, F. A. *J. Biol. Inorg. Chem.* **2003**, *8*, 787.
(37) Salerno, J. C.; Leigh, J. S. *J. Am. Chem. Soc.* **1984**, *106*, 2156.
(38) Walker, F. A.; Huynh, B. H.; Scheidt, W. R.; Osvath; S. R. *J. Am. Chem. Soc.* **1986**, *108*, 5288.
(39) Walker, F. A.; Nasri, H.; Turowska, I.; Mohanrao, K.; Watson, C. T.; Shokhirev, P. G.; Debrunner, P. G.; Scheidt, W. R. *J. Am. Chem. Soc.* **1996**, *118*, 12109.

Comparison of $(Py)_2Fe^{III}$(OEPO) and $(1\text{-MeIm})_2Fe^{III}$(OEPO). The data reported here indicate that $(Py)_2Fe^{III}$(OEPO) exists in the high-spin form throughout the temperature range 10−300 K. In contrast, $(1\text{-MeIm})_2Fe^{III}$(OEPO) undergoes a spin-state change from $S = 1/2$ to $S = 5/2$ (or spin admixed $S = 5/2, 3/2$) upon warming. In the solid state, both complexes crystallize with the iron at a center of symmetry. Thus, the axial ligands are parallel to one another in a plane that lies nearly directly over one of the trans N−Fe−N groups. Crystals of $(Py)_2Fe^{III}$(OEPO) and $(1\text{-MeIm})_2Fe^{III}$(OEPO) are isostructural, that is, they crystallize in the same space group and have similar cell dimensions. Consequently, the crystal environment does not impede $(Py)_2Fe^{III}$(OEPO) from undergoing the change in spin state seen for $(1\text{-MeIm})_2Fe^{III}$(OEPO). The preference of $(Py)_2Fe^{III}$(OEPO) for the high-spin state is determined by the lower basicity of pyridine (pK_a, 5.28) versus 1-methyl imidazole (pK_a, 7.20)[40] and the larger size of the six-membered ring in pyridine over that of the five-membered ring of 1-methyl imidazole. Both factors contribute to produce a lower ligand field strength for pyridine and a high-spin ground state for $(Py)_2Fe^{III}$(OEPO).

Comparison of $(Im)_2Fe^{III}$(OEPO) and $(1\text{-MeIm})_2Fe^{III}$(OEPO). At low temperature, these two complexes exist in the low-spin Fe(III) form and both show rhombic EPR spectra with similar g values. However, there are important differences in their geometric structures. In $(1\text{-MeIm})_2Fe^{III}$(OEPO), the axial imidazole ligands reside in parallel planes and the porphyrin is planar. In contrast, in $(Im)_2Fe^{III}$(OEPO) the axial ligands are in nearly perpendicular planes and the porphyrin has a sizable ruffled distortion. Frequently, steric interactions between the axial ligands and porphyrins have been assumed to be responsible for the perpendicular orientation of axial ligands in low-spin Fe(III) hemes.[23] However, in the cases of $(Im)_2Fe^{III}$(OEPO) and $(1\text{-MeIm})_2Fe^{III}$(OEPO), the steric requirements of the axial ligands are similar, and these cannot be responsible for the differences in observed structures. It is possible that the differences in solid-state structures result from the hydrogen-bonding interactions that are present in $(Im)_2Fe^{III}$(OEPO) but are absent in $(1\text{-MeIm})_2Fe^{III}$(OEPO). These interactions directly involve the axial ligands, and a perpendicular arrangement of these ligands clearly allows the extended pattern of hydrogen bonds shown in Figure 7 to exist. Note also that the same pattern of hydrogen bonds is seen in the two different solvates, **(**$Im)_2Fe^{III}$(OEPO)·2THF and **(**$Im)_2Fe^{III}$(OEPO)·1.6$CHCl_3$. The distortion of porphyrin cores is frequently associated with the presence of a perpendicular arrangement of the two, planar, axial ligands in low-spin Fe(III) hemes. Similar distortions of the macrocycle are seen in **(**$Im)_2Fe^{III}$(OEPO)·2THF and **(**$Im)_2Fe^{III}$(OEPO)·1.6$CHCl_3$, but steric interactions between the porphyrin and axial ligands are not likely to be responsible for this ruffling. Rather, the electronic structure of the iron may play a role with the dπ (d_{xz} and d_{yz}) orbitals becoming nearly degenerate in energy, a situation that is frequently associated with significant distortions of the porphyrin from planarity.[23]

Despite the differences in their structures, both $(Im)_2Fe^{III}$(OEPO) and $(1\text{-MeIm})_2Fe^{III}$(OEPO) show rhombic EPR spectra. With 4-fold symmetric porphyrins, the observation of a rhombic EPR spectrum for a low-spin Fe(III) complex with two planar axial ligands is indicative of a parallel orientation of the axial ligands. However, with $(Im)_2Fe^{III}$(OEPO) the macrocycle no longer has 4-fold symmetry, and consequently, this complex with its perpendicular axial ligand planes has the appropriate symmetry to display a rhombic spectrum. Thus, for mono meso substituted porphyrins, the observation of a rhombic EPR spectrum cannot be taken to indicate that the axial ligands are in parallel orientations.

Both complexes also show temperature-dependent increases in their magnetic moments which are likely to result from occupation of an $S = 5/2$ or spin admixed $S = 5/2, 3/2$ state at higher temperatures.

Experimental Section

Materials: Iron(III)octaethylporphyrin chloride was purchased from Mid Century. Samples of $Fe_2^{III}(OEPO)_2$ were prepared by an established route.[14]

Preparation of $(Py)_2Fe^{III}$(OEPO). Under an atmosphere of purified dinitrogen, 50 mg (0.043 mmol) of $Fe_2^{III}(OEPO)_2$ was dissolved in 10 mL of dioxygen-free pyridine. The mixture was stirred for 5 min to form a deep green-brown solution. This solution was filtered to remove any solid residue, and then the volume of the solution was reduced to one-fourth under reduced pressure. Dioxygen-free diethyl ether was carefully layered over the solution in a dinitrogen-filled glovebox. On standing for 3−4 weeks, dark blue crystals of the product formed. The crystals were collected by filtration, washed with diethyl ether, and vacuum-dried: yield 30 mg, 48%. Spectroscopic and magnetic measurements were made on samples obtained from large, carefully selected crystals of this complex.

Preparation of $(Im)_2Fe^{III}$(OEPO)·2THF. Under an atmosphere of purified dinitrogen, 50 mg (0.74 mmol) of imidazole was added to a suspension of 50 mg (0.043 mmol) of $Fe_2^{III}(OEPO)_2$ in 10 mL of dioxygen-free tetrahydrofuran. The mixture was stirred for 5 min to form a dark solution. The resulting solution was filtered to remove any solid residue. Subsequently, the volume of the solution was reduced to one-fourth under reduced pressure. Dioxygen-free *n*-hexane was then carefully layered over the solution in a dinitrogen-filled glovebox. On standing 4 or 5 days, dark red crystals of the product formed. These were collected by filtration, washed with *n*-hexane, and vacuum-dried: yield 44.4 mg (70%). UV/vis spectra (under N_2 atmosphere) in dichloromethane with 1% imidazole (λ_{max}, nm (ϵ, M^{-1} cm^{-1})): 398(2.6×10^4), 450 (2.0×10^4), 662 (1.6×10^4). Crystals of **(**$Im)_2Fe^{III}$(OEPO)·1.6$CHCl_3$ were obtained in a similar fashion from chloroform solution. Spectroscopic and magnetic measurements were made on samples obtained from large, carefully selected crystals of these complexes.

X-ray Data Collection. Crystals of the two complexes were obtained directly from the preparations as described above. The crystals were coated with a light hydrocarbon oil and mounted in the 90 K dinitrogen stream of a Bruker SMART 1000 diffractometer equipped with CRYO Industries low-temperature apparatus. Intensity data were collected using graphite-monochromated Mo Kα radiation. Crystal data are given in Table 2. Intensity data for

(40) Schoefield, K. *Hetero-aromatic Nitrogen Compounds*; Plenum Press: New York, 1967; p 146.

$(Py)_2Fe^{III}$(OEPO) at 10 K were collected on a Bruker Apex2 diffractometer equipped with a CRYO Industries low-temperature device.

Solution and Structure Refinement. Scattering factors and correction for anomalous dispersion were taken from a standard source.[41] An absorption correction was applied.[42] The solution of the structure was obtained by direct methods with SHELXS-97 and subsequent cycles of least-squares refinement on F^2 with SHELXL-97.

Instrumentation. The X-band EPR spectra were recorded on a Bruker ECS-106 instrument equipped with an Oxford Instruments variable-temperature liquid helium cryostat. The microwave frequency was measured by using a calibrated cavity resonator, and the magnetic field intensity was checked using solid DPPH as a standard. Magnetic susceptibility data were collected on a Quantum Design MPMS superconducting quantum interference device (SQUID) magnetometer with a 7-T superconducting magnet. The data were collected and analyzed through the use of a Design Magnetic Property Measurement System (MPMS) MultiVu software.

Voltammetric experiments were performed on a BAS CV-50W potentiostat with a three-electrode cell. A 1.5-mm-diameter Au disk electrode from Bioanalytical Systems, Inc. was used as the working electrode. Prior to experiments, the Au electrode was polished with fine carborundum paper and, then with a 0.5-μm alumina slurry. Subsequently, the electrode was sonicated in water in order to remove traces of alumina from the gold surface, washed with water, and dried. A silver wire immersed in 0.010 M $AgClO_4$, 0.09 M TBAP, in acetonitrile and separated from the working electrode by a "thirsty glass" tip of Bioanalytical Systems, Inc. served as the reference electrode. For this reference electrode, the ferrocene/ferrocenium formal redox potential was +220 mV. A Pt tab with a surface area of about 0.5 cm^2 served as the counter electrode.

Acknowledgment. We thank the NIH (Grant No. GM-26226, A.L.B.) for support and the NSF (Grant No. OSTI 97-24412) for partial funding of the 500 MHz NMR spectrometer.

Supporting Information Available: X-ray crystallographic files in CIF format for $(Py)_2Fe^{III}$(OEPO) (at 10 and 90 K), $(Im)_2Fe^{III}$(OEPO)·2THF, and $(Im)_2Fe^{III}$(OEPO)·1.6 $CHCl_3$. This material is available free of charge via the Internet at http://pubs.acs.org.

IC0607033

(41) *International Tables for Crystallography*; Kluwer Academic Publishers: Dordrecht, The Netherlands, 1992.
(42) Sheldrick, G. M. *SADABS*; University of Göttingen: Göttingen, Germany, 2003.